Synthesis of Biodegradable Cell-laden Microgels Assembly by Stop-Flow Lithography

Jakub Zlatník, Eliška Pazderková, Alina Mamedova, Jindřich Kropáček, Mario Rothbauer, Zdeněk Slouka, Ondřej Kašpar, Viola Tokárová*, Ivan Řehoř*

***Abstract*—This study presents a novel approach for the synthesis of biodegradable cell-laden microgels using stop-flow lithography (SFL), addressing critical challenges in the field of tissue engineering. Traditional methods for creating 3D cell cultures often rely on non-biodegradable materials, which limit their application and raise concerns about cell viability. In this work, we successfully replace poly(ethylene glycol) diacrylate (PEGDA) with dextran-2-hydroxyethyl methacrylate (dex-HEMA), a biocompatible and biodegradable alternative. Furthermore, we introduce a technical solution for sterile cell encapsulation, validated through assessments of cell growth and viability alongside the biodegradation rate of the microgel matrix. Our results demonstrate the potential of the self-assembly technique to form organized structures with high spatial resolution. By encapsulating relevant cell lines, Caco-2 and HT-29, within distinct microgel types, we pave the way for the development of sophisticated 3D co-culture models. These advancements hold significant promise for replicating the structural and functional complexities found in native tissues, thereby enhancing the relevance of in vitro studies in biomedical research.**

***Index Terms*—biodegradation, cell encapsulation, dex-HEMA, microgel, multicellular assembly, stop-flow lithography.**

This work was financially supported by the Grant Agency of the Czech Republic (GACR, no.: 23-05908K), the Ministry of Education, Youth and Sports of the Czech Republic (no.: CZ.02.01.01/00/22_008/0004597 – project Talking microbes - understanding microbial interactions within One Health framework), and by the grant of Specific university research (A1_FCHI_2025_004). Asterisk indicates corresponding authors; Viola Tokárová, Ivan Řehoř. Jakub Zlatník and Eliška Pazderková contributed equally to this work.

Jakub Zlatník, Eliška Pazderková, Alina Mamedova, Jindřich Kropáček, Zdeněk Slouka, Ondřej Kašpar, *Viola Tokárová, and *Ivan Řehoř are with the Department of Chemical Engineering, University of Chemistry and Technology Prague, Technická 5, Prague, 166 28, Czech Republic (e-mail: zlatnikj@vscht.cz, pazderke@vscht.cz, mamedova@vscht.cz, kropacej@vscht.cz, sloukaz@vscht.cz, kasparo@vscht.cz, tokarovv@vscht.cz, rehori@vscht.cz)

Mario Rothbauer is with the Department of Orthopedics and Trauma-Surgery, Medical University of Vienna, Währinger Gürtel 18-20, Vienna, 1090, Austria (e-mail: mario.rothbauer@meduniwien.ac.at).

I. Introduction

STUDYING living cells in a laboratory requires providing the cells with conditions similar to those encountered in their native environment. Although challenging, mimicking such an environment is at the forefront of scientific efforts. The challenge comes with the necessity of growing cells as 3D cultures, since well-established 2D cell cultures are known to alter cell behavior. In a 3D layout, cells can interact with other cells and the extracellular matrix (ECM), closely resembling a tissue environment. Several strategies have been developed to create 3D cell cultures [1]. Some methods manipulate the individual cells, assembling them into spheroids and organoids. The size of created spheroids and organoids is intrinsically limited to approximately 100-500 µm due to slow (diffusional) nutrient transport to their centers [2]. Other approaches utilize biocompatible materials that serve as scaffolds and microenvironments for the cells. Hydrogels are especially suitable matrices because they aid diffusion and can be designed to replicate key ECM characteristics such as mechanical stiffness, surface charge, cell affinity, and biodegradability. Therefore, cell-laden gels used for 3D cultures show significant potential in tissue engineering. However, the top-down techniques frequently employed for creating such constructs, such as electrospinning or bioprinting, often do not achieve the necessary spatial resolution, cell density, or cell arrangement that are present in native tissues [3].

Bottom-up approaches, working with (cell-laden) gel micro-objects (microgels), assemble the micro-objects into organized structures in a controlled way [1, 4, 5]. Such methodologies comprise self-assembly [6-8] and direct-assembly methods [9, 10]. Self-assembly refers to a process in which the microgel ensemble minimises its free energy, forming an organized structure. In contrast, direct-assembly involves the application of external forces to precisely manipulate and position microgels according to experimental requirements. Using both approaches, one can relate the complexity and resolution of the building blocks (microgels) to those of the final construct [11].

The fabrication of microgels with complex, arbitrary geometries predominantly employs lithographic microfabrication techniques such as photolithography and imprint lithography [12]. Stop-flow lithography (SFL) is a continuous photolithographic process conducted within microfluidic channels, known for its superior production rates, reaching up to 10^6 microgels per hour [13]. Such high

throughput capability makes SFL an excellent candidate for the synthesis of cell-laden microgels [14]. In fact, the production of cell-laden microgels via SFL has already been reported [5, 9, 15]; unfortunately, the gels contained non-biodegradable poly(ethylene glycol) diacrylate (PEGDA), limiting the application of such constructs and raising concerns about the fate of encapsulated cells. Also, the encapsulation of cells under sterile conditions continued to be an unresolved issue.

This work addresses the key challenges related to the practical SFL fabrication of cell-laden microgels discussed in the previous paragraph. Through a step-by-step optimization process, we show that PEGDA, as a non-degradable synthetic polymer, can be successfully replaced with a biocompatible and biodegradable dextran 2 hydroxyethyl methacrylate (dex-HEMA). At the same time, we provide a technical solution that enables sterile cell encapsulation, verified by monitoring cell growth, viability, and the biodegradation rate of the microgel matrix. Next, we demonstrate self-assembly and direct-assembly of individual cell-laden microgels to complex structures with high spatial resolution (Fig. 1A). Finally, two cell lines, Caco-2 and HT-29, which are relevant for modelling the cellular environment of the intestinal barrier [16], were encapsulated in two different types of microgels (Fig. 1B). This work thus marks a significant step forward in the high-throughput production of biocompatible cell constructs with considerable application potential. For instance, cell type-specific microgels can serve as a standardised set of fundamental building blocks, enabling the assembly of complex 3D co-culture models that reflect both the structural and functional complexity of various tissues. Consequently, these models might be a viable alternative to animal testing in the near future.

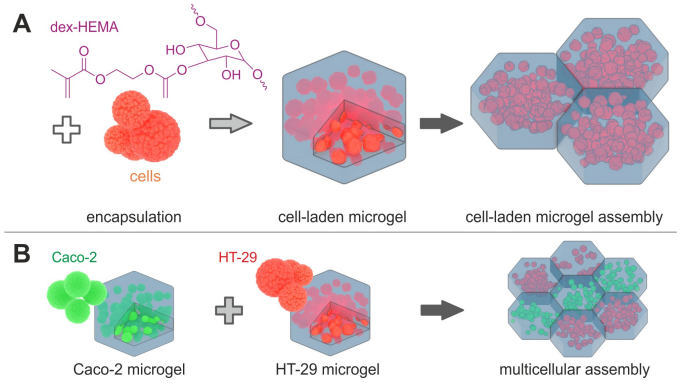

Fig. 1. A) The concept of forming cell-laden microgels from dex-HEMA and their assembly into larger aggregates; B) Preparation of multicellular assembly proposed in this work (Caco-2 and HT-29 cell lines).

II. Materials and Methods

A. Materials

The following chemicals with specified vendor and product numbers have been used throughout the research.

- Dulbecco's modified Eagle's medium with high glucose content (DMEM) – Sigma D6429
- Fetal bovine serum (FBS) – Sigma F7524
- MEM Non-essential Amino Acid Solution (100x) (NEAA) – Sigma M7145
- Penicillin-streptomycin antibiotics (PSA) – Sigma A5955
- Phosphate-buffered saline (PBS) – Sigma P4417
- Trypsin (Tryp) – Sigma T4799
- Ethylenediaminetetraacetic acid (EDTA) – Sigma 4005-OP
- Trypan Blue 0.4% (TB) – ThermoFisher Scientific 15250061
- LIVE/DEAD Viability/Cytotoxicity Kit (Assay solution) – ThermoFisher Scientific L32250
- Dextran (15 kDa) – Sigma 31387
- Lithium phenyl-2,4,6-trimethylbenzoylphosphinate (LAP) – Sigma 900889
- Pluronic® F-127 – Sigma P2443
- Dimethyl sulfoxide (DMSO) – Sigma 472301
- Fluorescein O-methacrylate (FOM) – Sigma 568864
- 2-Hydroxyethyl methacrylate (HEMA) – Sigma 477028
- Polydimethylsiloxane (PDMS) – Farnell 101697
- Sylgard 184 elastomer – Farnell 101697

Dextran was modified with HEMA to form the photoresponsive polymer dex-HEMA, following previously described protocols [17, 18]. The degree of substitution (DS) was determined to be 20 by ^{1}H-NMR spectroscopy. The microfluidic chips were made from PDMS elastomer prepared in a 1:10 weight ratio (curing agent to PDMS base).

B. Cell Cultivation and Handling

The HT-29 cell line was cultured in petri dishes (ø 10 cm) using DMEM solution (10% FBS and 1% PSA). The cultures were grown in an incubator at 37 °C under controlled conditions, i.e. 5% CO2 atmosphere with 95% humidity. A 25-minute trypsinisation was carried out using 2 ml of a 1:1 mixture of Tryp and EDTA at 70-80% cell confluency, typically after 3 days of incubation, prior to cell harvesting and subculturing. Before trypsinization, non-adherent cells were removed with 10 ml of PBS. During trypsinization, 4 ml of DMEM solution was added to resuspend and passage detached cells. A portion of the cells was incubated in 10 ml of fresh DMEM solution.

Caco-2 cells were cultured under conditions comparable to those used for HT-29, with slight variations in culture vessels and medium composition. Specifically, the Caco-2 cell line was maintained in T-75 flasks using DMEM supplemented with 10% FBS, 1% NEAA, and 1% PSA. The cells were incubated at 37 °C in a 5% CO_2 atmosphere with 95% humidity. Subculturing was performed upon reaching 80% confluency using a 1:1 Tryp/EDTA solution, following the same protocol as for HT-29 cells. Cell harvesting followed the same procedures outlined for the HT-29 cell line.

The harvested cells for gel encapsulation were counted using a hemacytometer. Dead cells were indicated by staining with TB. The preparation of cells for counting was performed as follows: (i) cells resuspended in DMEM solution were centrifuged at 250 g for 3 minutes, (ii) the supernatant was aspirated, and the cell pellet was resuspended in fresh DMEM solution (5 ml), (iii) 10 µl of cell suspension was mixed with 10 µl of TB, and the resulting mixture was used for cell counting.

The viability test of the encapsulated cells using the LIVE/DEAD assay involved incubating 200 µl of gel-encapsulated cells with staining solution in a 96-well plate for 30 minutes, which differentiated live and dead cells by colour, and visualising them on an Olympus IX81 inverted microscope with a FluoView FV1000 confocal system and a 40x objective.

C. Pre-gel Preparation

Before use, all solid chemicals were sterilised in an autoclave at 121 °C for 30 minutes, and liquid solutions were filtered through 0.22 µm sterile syringe filters. The prepared PDMS microfluidic device was sterilised with 70% ethanol. All other equipment and working surfaces were exposed to UV light.

The pre-gel solution was prepared as a mixture of dex-HEMA, LAP, and cell pellets. The tested concentrations ranged from 0.05% to 0.35% (w/w) for LAP and 20% to 40% (w/w) for Dex-HEMA. The composition of the pre-gel was 35% (w/w) dex-HEMA, 0.1% (w/w) LAP in the cell medium. Firstly, 40 mg of dex-HEMA was dissolved in 60 µl of DMEM solution, followed by filtration through a 0.22 µm syringe filter to remove any potential biological contaminants. The loss during filtration was measured by weighing the filtered solution, typically yielding around 50 mg of sample. The LAP solution was prepared by dissolving 5 mg of LAP in 58 µl of cell medium, then filtered through a 0.22 µm syringe filter. Adding 7 µl of the LAP solution to the dex-HEMA solution yielded dex-HEMA and LAP concentrations of 35% and 0.1% (w/w), respectively. Other concentrations of dex-HEMA and LAP tested in the study were prepared similarly, only with modified component concentrations.

D. Cell Encapsulation

In the next step, the pre-gel solution was combined with the specified amount of cell pellet. Given the thorough removal of the cell culture supernatant by aspiration, it can be assumed that adding cells does not cause noticeable dilution of the pre-gel solution. Investigated *v/v* ratios of the cell pellet, i.e., cells free of supernatant, to the pre-gel solution were 1:9, 1:4 and 1:1. Finally, the pre-gel-cell mixture was gently homogenised using a pipette tip. In some experiments, microgels were also fluorescently labelled by adding a solution of FOM prepared in DMSO with a final FOM concentration in the pre-gel of 0.07% (*w/w*).

E. Cell-laden Microgels Fabrication Using SFL

The PDMS microfluidic chips used for the SFL process were fabricated following a previously reported protocol [16]. The overall layout of the device is shown in Fig. 2. The whole experiment was carried out in a sterile flow box, and all media were heated to 37 °C. The microfluidic chip (Fig. 2(A)) was rinsed with DMEM solution, and 30 to 50 µl of pre-gel was pipetted into the microfluidic chip inlet (Fig. 2(C)). A collection Eppendorf tube (Fig. 2(F)), prefilled to 80% with DMEM solution containing 0.1% Pluronic® F-127 (*w/w*), was connected to the microfluidic chip outlet (Fig. 2(E)). To prevent any contamination, the microfluidic chip was assembled inside an air-tight box with transparent top and bottom glass windows. Next, a carrier gas supply (N_2) was connected, and the sealed box was mounted on the platform of a Nikon Eclipse Ti-2 inverted microscope.

Flow setup. The flow rate of carrier gas, and thus the flow rate of pre-gel in the microfluidic channel, was regulated using a pressure-reducing valve. The carrier gas was also responsible for repeating the three-step sequence of the SFL process: flow cessation, photo-polymerisation, and flow resumption. In the first step, the carrier gas inlet is closed with a three-way valve, halting the flow of pre-gel solution within the microfluidic channel (Fig. 2(D)). Next, the focused region of the channel is illuminated, causing the polymerisation of areas defined by the photomask design. Finally, the carrier gas is reintroduced, restarting the flow of the prepolymer solution and enabling the transport of newly formed microgels from the illumination area towards the outlet reservoir (Fig. 2(F)).

Illumination setup. Radiation from an X-Cite 200DC lamp illuminator (340-800 nm) was reflected to the sample using 420 nm longpass dichroic mirror, placed in the position of the fluorescent cube, while the sample was simultaneously observed using diascopic imaging. Light of lower wavelengths passed through the photomask and polymerized pre-gel solution only in the mask-defined region of the microfluidic channel to form cell-laden microgel particles. The radiation intensity at the illuminator was adjustable from 0% to 100% (equal to 200 W).

Process control. The control of the alternating illumination and flow regimes in the microfluidic channel was provided by dedicated automatic system [19] with the following adjustable parameters: (i) illumination time, (ii) waiting time between illumination and flushing, (iii) flushing time, and (iv) waiting time between flushing and illumination (parameters ranging from 100 to 1000 ms). The production rate of this setup was typically 10,000 microgel particles per hour.

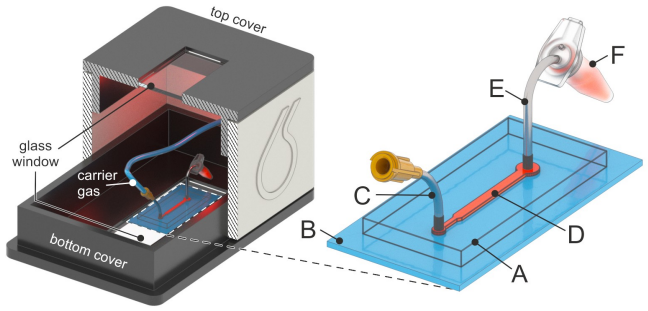

Fig. 2. Scheme of the sterile box (cross-section) and PDMS chip used for the SFL process: A – PDMS chip (wireframe), B – glass slide with a thin PDMS layer, C – inlet port, D – SFL channel (height - 50 µm. width - 400 µm, length - 2500 µm), E – outlet port, F – attached Eppendorf tube with perforated lid for collecting microgels.

Microgel handling. The cross-linked microgels were collected and washed 16 times with cell culture medium to remove any residual unreacted polymer, photoinitiator, and, most importantly, non-encapsulated cells. The removal of non-encapsulated cells relied on different sedimentation rates of microgels and cells: a brief, 1-minute gravity-driven

sedimentation allowed microgels to be collected at the bottom of the vial, leaving free cells suspended in the solution. After washing, the microgels were pipetted into a sterile 96-well plate and kept in an incubator. The growth medium was replaced daily throughout the entire observation period to maintain optimal cell culture conditions.

F. Degradation Rate of dex-HEMA

Multiple factors, including the initial composition of the pre-gel, the parameters of the SFL process, and the incubation environment, influence the rate at which the hydrogel matrix degrades. In this study, we examined how two key SFL parameters, i.e., (i) exposure time and (ii) light intensity, affect the biodegradation of gels formed from a pre-gel consisting of 40% dex-HEMA, 0.1% LAP, and 2% FOM (w/w).

Specifically for the degradation rate study, five distinct microgel morphologies were synthesised: triangular, hexagonal, stretched hexagonal, pentagonal, and square. Each shape was linked to a unique set of exposure conditions. This method enables us to simultaneously investigate the degradation rates of all morphologies and easily distinguish between all microgel types.

A mixture of cell-free microgels of various shapes was then monitored for their degradation rates during storage in an incubator set at 37°C with a 5% CO2 atmosphere and 95% humidity, in DMEM medium. Degradation was evaluated through changes in swelling behaviour and fluorescence decline, measured via image analysis using ImageJ [20]. Swelling was quantified as the percentage change in a selected linear dimension of each particle. The reduction in fluorescence signal with respect to background, indicative of progressive microgel erosion, was represented by the average grey value (8-bit image) within the boundary region of each particle type. Measurements were taken daily using a fluorescence microscope until the particles were entirely disintegrated.

G. Self-assembly and Bonding of Microgels

To evaluate the self-assembly and bonding abilities of microgel particles with different cell contents, two types of dex-HEMA-based hexagonal microgels were produced. The first type, containing HT-29 cells, was labelled with fluorescein O-methacrylate (FOM) to enable straightforward identification. The second type (not fluorescently labelled) contained encapsulated Caco-2 cells. Equal amounts of both microgel types were pipetted into individual wells of a 96-well plate with a U-shaped bottom geometry. Due to the curved bottom and gravitational forces, the microgel particles gradually concentrated at the centre of the well bottom, leading to geometry-induced self-assembly. To achieve permanent bonding between individual microgels forming aggregates, the culture medium was carefully replaced with a low concentration solution of PEGDA (2.5%, w/w) containing LAP (1%, w/w) as the photoinitiator. The assembled microgels were then exposed to a collimated, low-intensity UV light beam focused on the points of contact between individual microgel pairs.

III. Results and discussion

A. Optimization of Pre-gel Composition

In the initial phase, the optimization of gel synthesis parameters for SFL was the primary focus. The prepared microgels, however, must also provide a suitable environment for the encapsulated cells, restricting the possible synthetic conditions. Since the viability of encapsulated cells depends primarily on pre-gel composition and gelation process, a systematic investigation was conducted to assess the impact of (i) pre-gel composition, including photoinitiator and dex-HEMA concentrations as well as cell loading, (ii) exposure time, and (iii) the irradiation intensity on cell viability and gel degradation dynamics.

LAP (lithium phenyl-2,4,6-trimethylbenzoylphosphinate), used here as a photocrosslinker, has a potential cytotoxic effect on cells [21, 22]. A previous study showed an adverse effect of hydrogel extract (10% methacryloyl gelatin and 0.1 to 1% w/w LAP) on the viability of human primary renal proximal tubule epithelial cells (hRPTECs) [21]. Therefore, it is crucial that the LAP concentration in the pre-gel solution does not exceed several hundredths to tenths of wt%. At the same time, its concentration shall ensure the synthesis of a sufficiently strong hydrogel matrix. To evaluate the appropriate LAP concentration, we synthesized hydrogel particles with a fixed dex-HEMA concentration of 30% (w/w) and different LAP concentrations of 0.050, 0.078, 0.100, 0.250, 0.300, and 0.350% (w/w). Although it was possible to reach the gelation point in all cases, the edges of the hydrogel particles were blurred when using LAP concentrations lower than 0.1% w/w. This observation established a minimum LAP concentration of 0.1% w/w, allowing SFL synthesis of hydrogel particles with well-defined shapes. As the LAP content exceeded 0.3%, the high number of initiation centers of the photopolymerization reaction in the pre-gel resulted in an increased tendency of the synthesized gels to stick to the surface of the microchannel, making continuous SFL not feasible. The stickiness was most likely caused by the excessive depletion of oxygen from the inhibition layer, as previously described by Dendukuri et al. [23, 24]. Based on all previous findings, the suitable LAP concentration was identified within the range of 0.1 to 0.3% (w/w) in the pre-gel solution. This concentration range ensures robust and fault-free synthesis of hydrogel particles with non-distorted, sharp edges and well-defined footprints.

Next, the effect of dex-HEMA concentration was investigated. Dex-HEMA is available in several variants, differing in DS and molecular weight. These properties affect pre-gel density and viscosity and the final properties of the formed hydrogel particles, especially crosslinking density reflected in the concomitant degree of swelling [25], Young modulus, or perfusivity. Based on our previous results [18], we selected 15-kDa dex-HEMA with a DS of 20 as an optimal carrier material. The dex-HEMA concentrations of 20, 30, 35, and 40% (w/w) were tested while maintaining LAP concentration at 0.2% (w/w). The dex-HEMA content of 40% provided a highly viscous pre-gel that required the application of higher pressures of the carrier gas during the SFL process. Unfortunately, the use of high pressures repeatedly resulted in

damage to the PDMS microfluidic device. Furthermore, the high viscosity of the pre-gel did not allow sterilization by simple filtration through a 0.22 µm filter, and therefore, 40% concentration of dex-HEMA was not further considered for practical reasons. The lower dex-HEMA content, i.e. 30% to 35%, was preferred for the SFL process. Another lowering of dex-HEMA concentration, specifically to 20%, yielded a sufficiently crosslinked hydrogel matrix capable of withstanding degradation during incubation over several days. However, this concentration was not suitable for cell encapsulation, as shown in the next section.

The elastic (Young) modulus of the dex-HEMA was measured with the TI 950 TriboIndenter (Bruker Corp.) instrument, and the value of 16.3 ± 2.0 kPa was observed, which is within the range of soft tissues [18].

B. Degradation of Microgels

The connections between the dextran backbone and the HEMA moieties, used as crosslinks, are realized via hydrolytically labile carbonate ester bonds [26]. Hence, the synthesized microgels spontaneously degrade in the solution up to the point when they dissolve completely. The gel degradation time depends on the cross-linking density, which is heavily affected by the gelation process. Therefore, we evaluated the impact of two parameters of the SFL synthesis on the gel degradation rate – the UV exposure intensity and exposure time. Although these two parameters are connected, their relation is not trivial. The density of gel crosslinks is not a simple function of the light dose due to the variable termination rate, as the termination rate depends on the instantaneous radical concentration during the gel formation. High exposure intensities correlate with high initiation rates, producing relatively high radical concentrations. At the same time, a short radical lifetime results in a high termination rate and, thus, lower degrees of polymerization. Lower exposure intensity has the opposite effect [27]. In the case of gelation, the evolution of the percolation length depending on the above-stated kinetic parameters needs consideration [28].

Since such an in-depth view into radical polymerization gelation is far beyond the scope of this study, we independently varied the two discussed exposure parameters, evaluating the degradation kinetics of the created gels. Notably, the exposure has two strict qualitative upper and lower limits. At the lower limit, no gelation occurs due to insufficient exposure. At the upper limit, the formed radicals diffuse out from the exposed area, causing unintended gelation of the unexposed pre-gel solution, resulting in larger microgels with blurred contours.

Two sets of experiments were conducted to investigate the effects of exposure time and exposure intensity on the gel degradation kinetics. In the first experimental set, we prepared gels at a constant exposure time of 500 ms and varied the exposure intensity (50, 75, and 100%). The second set produced gel particles at 100% exposure intensity with variable exposure times (190, 350 and 500 ms). The time-dependent degradation of the hydrogel particles was measured using two methods. The first method visually tracked the swelling of the particles over time, since the density of cross-links and equilibrium volume are connected [29]. The second method follows the gradual decrease in the fluorescence intensity of stained microgels. This decrease is directly related to hydrogel degradation and release of fluorescein O-methacrylate (FOM). Fig. 3A shows particles whose swelling was measured over a period of 8 days. Fig. 3B depicts particles over the same time interval, where gradual leaching of FOM occurs because of degradation. As mentioned earlier, each shape corresponds to a specific parameter setting (Table 1).

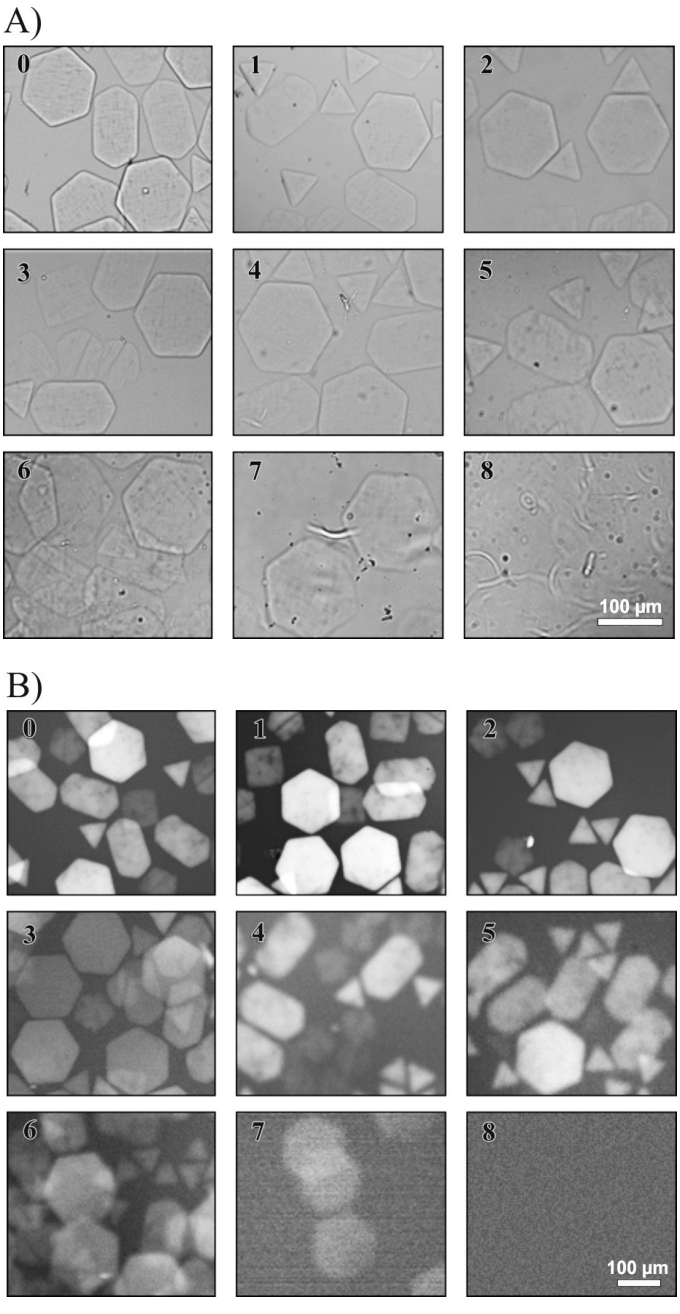

Fig. 3. A) Brightfield and B) fluorescence images showing the degradation of cell-free dex-HEMA-based microgels. Note: the number in the top left corner indicates days elapsed since fabrication.

This article has been accepted for publication in IEEE Transactions on NanoBioscience. This is the author's version which has not been fully edited and content may change prior to final publication. Citation information: DOI 10.1109/TNB.2025.3644496

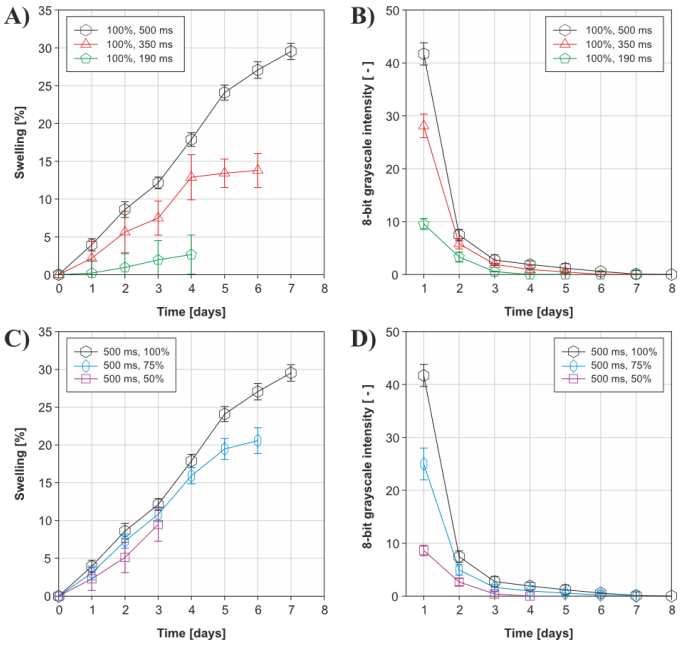

Fig. 4. Cell-free dex-HEMA-based microgels degradation time study: Swelling (A) and fluorescence intensity (B) of particles formed with variable illumination time (190, 350, and 500 ms) at 100% irradiation intensity; and swelling (C) and fluorescence intensity (D) of particles prepared at 500 ms illumination time and variable irradiation intensity (50, 75, and 100%).

The graphs in Fig. 4 illustrate the progression of degradation over time as average values of swelling (Fig. 4A, C) or the reduction in intensity of the encapsulated fluorescent dye (Fig. 4B, D), respectively. A microgel was considered completely degraded when its boundary could no longer be determined in a brightfield image and when it could not be distinguished from the background of the fluorescence image.

The obtained results of degradation are summarized in Table 1. The degradation times ranged from four to eight days, depending on the parameter settings. In general, the longer the exposure time, the longer it took for complete gel degradation. Similarly, higher exposure intensities resulted in longer degradation times. These lifetimes of the carrier gels align well with the proliferation rates of the encapsulated cells as described in the following section. If necessary, the degradation times can be extended beyond the upper limits indicated in Table 1 by varying the degree of substitution of dex-HEMA or by adding a small amount of non-degradable polymer such as dextran methacrylate [26].

TABLE I
DEGRADATION TIME VS EXPOSURE TIME AND INTENSITY

Particle shape	Exposure Time [ms]	Exposure Intensity [%]	Degradation Time [days]
Square	500	50	4
Stretched hexagon	500	75	7
Regular hexagon	500	100	8
Triangle	350	100	6
Pentagon	190	100	5

Particle composition - 40 wt% dex-HEMA, 0.1 wt% LAP. Note: 100% exposure intensity corresponds to 200W (X-Cite 200DC Mercury Vapor Short Arc lamp).

C. Cell Encapsulation

Initial experiments involving the encapsulation of HT-29 cells within a pre-gel matrix containing 20% (w/w) dex-HEMA indicated the need to use higher concentrations. The microgels made of 20% dex-HEMA were thinner (approx. 20 µm) compared to those made of 30% dex-HEMA (approx. 30 µm). This observation might be attributed to the presence of an oxygen inhibition layer near the top and bottom channel walls (made from PDMS permeable to oxygen), which inhibits radical polymerization [30]. Increasing the dex-HEMA content offers two main advantages for cell encapsulation: (i) a thicker microgel can accommodate a greater number of cells due to steric factors, and (ii) a denser gel matrix provides enhanced structural support, thereby reducing cell loss during washing and handling. It should also be noted that the influence of channel height was also considered. Reducing the channel height from 50 to 30 µm resulted in very poor cell encapsulation, as a significant number of cells (d ~ 10 µm) were only partially embedded in the gel matrix and, due to excessive exposure, were more likely to detach during handling. These results determine the final formulation of the pre-gel suitable for cell encapsulation, which includes 0.3% (w/w) LAP, 30 to 35% (w/w) of dex-HEMA, and utilises a 50 µm SFL channel.

The loading cell capacity of the gel was the following investigated parameter aimed at obtaining microgels with cells distributed uniformly within their volume. Several batches of cell-laden microgels were prepared, differing in cell-to-pre-gel volume ratios of 1:9, 1:4, and 1:1. To minimise the effect of gravity on cell sedimentation within the pre-gel and reduce variation in cell density along the z-axis in the final microgel, the gelation process occurred near the entrance of the SFL microfluidic channel (Fig. 2(D)).

In the case of the 1:9 ratio, we found a nonhomogeneous distribution of cells within the gel, forming localised clusters (Fig. 5A). We also observed loss of individual cells during the washing step (surface voids) due to their weak mechanical stability on the microgel surface. Interestingly, at a 1:1 volume ratio, the HT-29 cells relatively uniformly filled the gel volume and exhibited high mechanical stability and resistance to detachment. Unfortunately, an additional increase in cell concentration compromised the microgels' shape fidelity, which is essential for the assembly of multi-microgel aggregates (Fig. 5C).

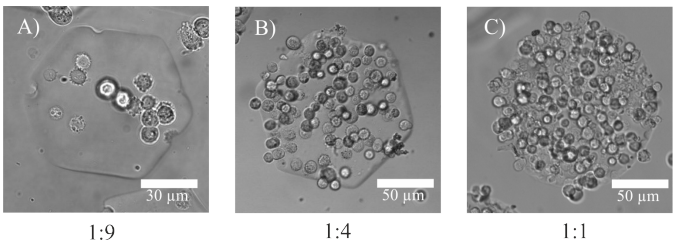

Fig. 5. Cell-laden microgel particles (HT-29) with different cells-to-pre-gel volume ratios: A) 1:9, scale bar (30 µm), B) 1:4, scale bar (50 µm), and C) 1:1, scale bar (50 µm).

To conclude, the microgels prepared at a 1:4 ratio contained a sufficient number of encapsulated cells with minimal loss during washing and incubation. At the same time, the original

footprint was preserved (Fig. 5B). We speculate that attractive cell-cell interactions, to some extent, contributed to preventing cell loss. Therefore, the 1:4 ratio was selected for the following cell growth experiments.

D. Growth and Viability of Encapsulated Cells

The viability of HT-29 cells was tested on cell-laden microgels prepared with the following concentrations and process parameters: 30% dex HEMA, 0.3% LAP, 0.07% FOM (w/w); 1:4 cell-to-pre-gel volume ratio; and 300 ms exposure time with 50% intensity. These values were chosen as a trade-off between observed gel degradation rate and cell viability, which was evaluated two hours and five days after exposure.

Fig. 6A and B show the brightfield image and confocal scan of the prepared microgel two hours after the exposure. The live and dead cells are labelled green and red, respectively, using the LIVE/DEAD Viability/Cytotoxicity Kit. Qualitatively, after the SFL process, the dead cell content is negligible. One also notices the uniform cell distribution in the xy-plane and along the z-axis of the hydrogel particle, as shown in Fig. 6B and Fig. 6C, respectively.

To evaluate the cell death solely caused by the SFL process, we counted the number of dead cells before and after encapsulation in the hydrogel. Staining the cells with trypan blue after trypsinization showed 5.4 ± 2.3 % dead cells. After encapsulation, the proportion of dead cells increased to 12.9 ± 5.2 %, as determined by confocal microscopy. The SFL encapsulation process is, thus, well tolerated by the HT-29 cell line despite the previous reports on the cytotoxic impact of the methacrylic acid formed by the reverse hydrolysis of the hydrogel matrix during particle incubation in aqueous DMEM solution [31, 32].

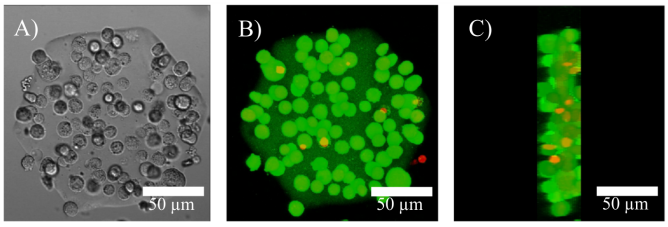

Fig. 6. A) Bright-field image of a microgel with encapsulated HT-29 cells. B) Top view of a cell-laden microgel on a confocal microscope. C) Side view of a cell-laden microgel on a confocal microscope. Scale bar (50 µm). Colors in B and C represent live (green, FOM) and dead (red) cells.

Observation confirmed that upon encapsulation, the HT-29 cells remained viable in the gel (Fig. 7A), and within several days (typically 3 to 4), the cells outgrew the gel particle (Fig. 7B). The characteristic times of overgrowth align with the observed times of gel degradation (within the period of 4 to 8 days). This shows that initially, the microgels firmly contain cells within a defined region, but later they allow the expanding cells to surpass the original microgel boundaries.

Although cells grow on both the top and bottom surfaces of the hydrogel support, they exhibit a preference for the bottom gel side, likely due to their adherent nature. This preference is clearly visible on the surface of the incubation well (Fig. 8). Compared to the bottom side, the growth on the top surface is relatively incremental. Fig. 8A shows the area of new cells growing on the top of the hydrogel support. While fully viable cells grow near and on top of the surface of the hydrogel particle, the center of the particle also contains dead cells (Fig. 8B). This phenomenon, likely caused by a limited nutrient or oxygen supply, can be mitigated through improved geometric design. Such a design should enhance mass transport of nutrients, oxygen, and waste removal by incorporating extra pores using soluble porogens in the pre-gel formulation or by adding perfused channels (along the z-axis) at sub-cellular scales to the original mask layout.

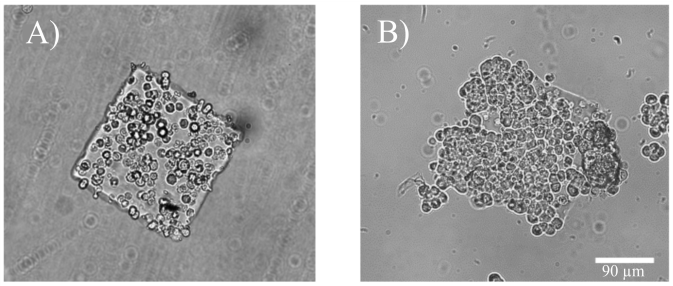

Fig. 7. A) Cell-laden microgel immediately after SFL, B) cell-laden microgel after 3 days of incubation showing proliferating cells growing from the decomposing particle.

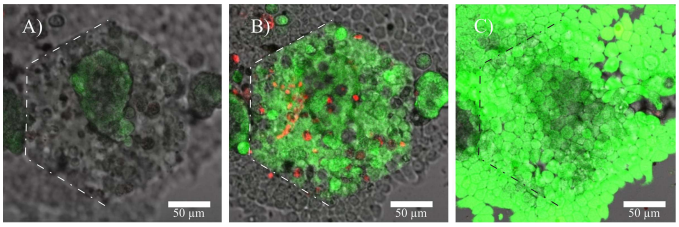

Fig. 8. Confocal microscopy images of a cell-laden microgel particle after 5 days of incubation in various focal points: A) above the top surface of the microgel particle (z = 0 µm); B) at the center of the microgel particle (z = 32 µm); C) at the bottom of the incubation dish below the microgel (z = 54 µm). Colours represent dead cells (red), live cells, and hydrogel marked by FOM (green).

E. Self-assembly of Microgels

Using round-bottom 96-well plates, Dex-HEMA-based microgels resuspended in the medium were observed to undergo gravitational settling, followed by sliding in a radial direction towards the lowest point of the well. This passive self-assembly process, which exploits wall curvature, has proven especially beneficial as it allows the spatial organisation of particles into larger, close-packed aggregates without any external intervention. Moreover, this method is straightforward, reproducible, and compatible with standard laboratory equipment that does not require specialised personnel.

This approach also enables co-localisation of particles with different properties (e.g., cell types, surface markers, mechanical stiffness), offering a straightforward route to form heterogeneous tissue-like constructs. In this study, we used a combination of HT-29-laden fluorescent microgels and Caco-2-laden non-fluorescent microgels to visually monitor the assembly process. The microgel particles were prepared with the following concentrations and process parameters: 30% dex-HEMA, 0.5% LAP, and 0.07% (w/w) FOM (only for

HT-29-laden particles), with a 450 ms exposure time at 40% intensity. The cell count per 1 µl of pre-gel was typically 1000 and 150 cells for HT-29 and Caco-2 microgels, respectively. Fig. 9 illustrates the typical outcome of the self-assembly process, where both microgel types are co-localised at the well centre in the course of a few minutes.

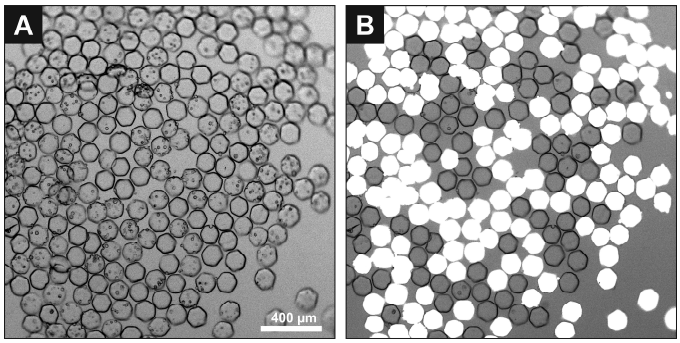

Fig. 9. Self-assembly of two types of cell-laden microgels (Caco-2 and HT-29) in a round-bottom 96-well plate. A) Bright-field image showing gravitational accumulation of microgel particles at the center of the well bottom; B) Fluorescence image indicating the presence of FOM-labelled HT-29-laden particles (bright), allowing visual distinction from non-labelled Caco-2-laden particles.

F. UV-induced Bonding of Microgel Assembly

To stabilise the self-assembled structures (discussed in the previous section) and turn them into permanent constructs, we replaced the culture medium with a low-concentration PEGDA solution containing LAP. When exposed to localised low-intensity UV light, the PEGDA polymerised at contact points between adjacent microgels, effectively bonding them together. The UV-induced bonding process and its progression are illustrated in Fig. 10 and Supplementary Movie SI1, showing the transition from individual particles to a fused structure.

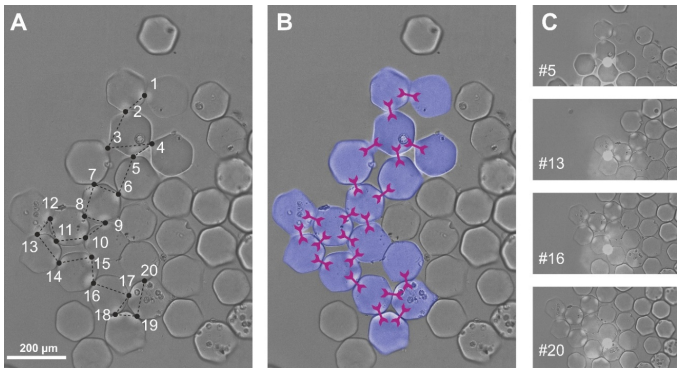

Fig. 10. The process of UV-bonding individual microgels into the assembled cluster – A) step-by-step process of UV illumination; B) bonded microgels with highlighted connection points; C) UV illumination (visible as the bright points) for specific connections of the assembly.

To verify the mechanical integrity of the bonded assemblies, the constructs were subjected to mechanical agitation by pipetting fresh medium into the well (Supplementary Movie SI2). As a result, the multi-microgel structure was temporarily detached from the well bottom. Upon sedimentation, it unfolded and retained its original shape as a single unit with no visible damage or broken connections, indicating structural integrity of the microgel assembly (Fig. 11). Therefore, it has been confirmed that the proposed methodology enables the fabrication of modular, multicellular units with a defined architecture and composition, thereby paving the way for the bottom-up assembly of larger tissue-like structures that can potentially serve as an alternative to *in vivo* testing.

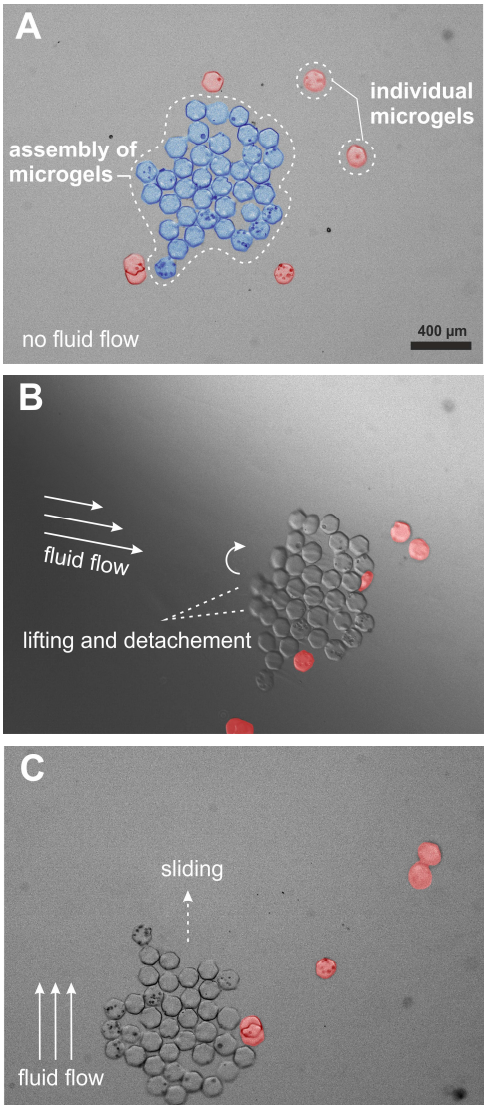

Fig. 11. Structural integrity of UV-bonded microgel assemblies: A) bright-field image of a self-assembled and UV-bonded cluster of microgel particles at the bottom of a round-bottom well; B) the same construct after mechanical disturbance by pipetting - the cluster is temporarily detached from the surface but retained its shape; C) the microgel assembly returned to the bottom of the well as a stable, intact unit, confirming successful PEGDA-mediated bonding.

IV. Conclusion

Targeting the 3D format of cell culturing, eventually leading to artificial tissues, we developed a method for sterilely synthesizing cell-laden microgels as primitive building blocks for assembling spatially precise tissue constructs. The method relies on high-throughput SFL

lithography applied to biocompatible and biodegradable dextran 2 hydroxyethyl methacrylate (dex-HEMA) as the principal component of the synthesized hydrogels. Our experimental studies provide optimal conditions for hydrogel preparation, complying with successful cell encapsulation and their growth. Specifically, the optimal gel consisted of 30% dex-HEMA added with LAP at the final concentration of 0.3% (w/w). Such pre-gel mixed with cell pellets at the volume ratio of 4:1 yielded, upon tuned exposure conditions, well-defined gel microparticles with encapsulated living cells. The gel microparticles spontaneously degraded in 4-8 days, depending on the exposure conditions, when stored in DMEM medium in the incubator at 37 °C. Importantly, such gel particles supported cell growth with characteristic times corresponding to those of the gel degradation times, clearly showing their potential use for creating larger cell constructs.

Furthermore, we demonstrated that microgel particles spontaneously undergo self-assembly in round-bottom wells, enabling the creation of organized multicellular aggregates. The ability to co-assemble particles containing different cell types introduces a versatile platform for building heterogeneous constructs. To stabilize these assemblies, we employed localized UV bonding using PEGDA as a secondary photopolymerizable matrix. The resulting constructs retained their shape even after mechanical disturbance, confirming the robustness of the bonding process. Together, these findings represent a significant step toward bottom-up fabrication of modular, functional tissue constructs with controllable geometry, composition, and degradation profile, highlighting the potential of SFL-generated dex-HEMA microgels for advanced applications in tissue engineering and regenerative medicine.

Acknowledgment

This work was financially supported by the Grant Agency of the Czech Republic (GACR, no.: 23-05908K), by a grant from the Programme Johannes Amos Comenius under the Ministry of Education, Youth and Sports of the Czech Republic (project no.: CZ.02.01.01/00/22_008/0004597), and by the grant of Specific university research (A1_FCHI_2025_004).

Author contributions

JZ and EP contributed equally to this work. IR – conceptualization and design of the project; VT, IR – project administration, supervision, funding acquisition; JZ, EP, AM, and JK – investigation and data curation; JZ, EP, AM, VT, ZS, OK, and MR – analysis of data, and visualization; and EP, IR, JZ, VT, ZS and JK – writing and editing of the manuscript.

Competing Interests

The authors declare no competing interests.

References

[1] S. Guven, P. Chen, F. Inci, S. Tasoglu, B. Erkmen, and U. Demirci, "Multiscale assembly for tissue engineering and regenerative medicine," Trends Biotechnol, vol. 33, no. 5, pp. 269-279, May, 2015.

[2] J. Kroupová, J. Hanuš, and F. Štěpánek, "Surprising efficacy twist of two established cytostatics revealed by a-la-carte 3D cell spheroid preparation protocol," Eur J Pharm Biopharm, vol. 180, pp. 224-237, Nov, 2022.

[3] Principles of Tissue Engineering, Amsterdam: Elsevier, Academic Press, 2020.

[4] Y. Morimoto, A. Y. Hsiao, and S. Takeuchi, "Point-, line-, and plane-shaped cellular constructs for 3D tissue assembly," Adv Drug Deliv Rev, vol. 95, pp. 29-39, Dec 1, 2015.

[5] T. Yue, M. Nakajima, M. Takeuchi, C. Hu, Q. Huang, and T. Fukuda, "On-chip self-assembly of cell embedded microstructures to vascular-like microtubes," Lab Chip, vol. 14, no. 6, pp. 1151-61, Mar 21, 2014.

[6] S. Xin, J. Dai, C. A. Gregory, A. Han, and D. L. Alge, "Creating Physicochemical Gradients in Modular Microporous Annealed Particle Hydrogels via a Microfluidic Method," Adv Funct Mater, vol. 30, no. 6, Feb 5, 2020.

[7] B. Zamanian, M. Masaeli, J. W. Nichol, M. Khabiry, M. J. Hancock, H. Bae, and A. Khademhosseini, "Interface-directed self-assembly of cell-laden microgels," Small, vol. 6, no. 8, pp. 937-44, Apr 23, 2010.

[8] K. Jakab, C. Norotte, F. Marga, K. Murphy, G. Vunjak-Novakovic, and G. Forgacs, "Tissue engineering by self-assembly and bio-printing of living cells," Biofabrication, vol. 2, no. 2, pp. 022001, Jun, 2010.

[9] W. Yang, H. Yu, G. Li, Y. Wang, and L. Liu, "High-Throughput Fabrication and Modular Assembly of 3D Heterogeneous Microscale Tissues," Small, vol. 13, no. 5, Feb, 2017.

[10] S. Tasoglu, C. H. Yu, H. I. Gungordu, S. Guven, T. Vural, and U. Demirci, "Guided and magnetic self-assembly of tunable magnetoceptive gels," Nat Commun, vol. 5, pp. 4702, Sep 1, 2014.

[11] T. P. Nguyen, F. Li, S. Shrestha, R. S. Tuan, H. Thissen, J. S. Forsythe, and J. E. Frith, "Cell-laden injectable microgels: Current status and future prospects for cartilage regeneration," Biomaterials, vol. 279, pp. 121214, 2021.

[12] M. E. Helgeson, S. C. Chapin, and P. S. Doyle, "Hydrogel microparticles from lithographic processes: novel materials for fundamental and applied colloid science," Curr Opin Colloid Interface Sci, vol. 16, no. 2, pp. 106-117, Apr 1, 2011.

[13] G. C. Le Goff, J. Lee, A. Gupta, W. A. Hill, and P. S. Doyle, "High-Throughput Contact Flow Lithography," Adv Sci (Weinh), vol. 2, no. 10, pp. 1500149, Oct, 2015.

[14] J. Kropacek, C. Maslen, B. van Dijk, A. Iniguez-Rabago, J. T. B. Overvelde, A. Zubov, J. Vrba, P. Cigler, F. Stepanek, and I. Rehor, "Hydrogel Microrobots Self-Assembled into Ordered Structures with Programmable Actuation," Advanced Intelligent Systems, vol. 5, no. 9, pp. 2300096, 2023.

[15] P. Panda, S. Ali, E. Lo, B. G. Chung, T. A. Hatton, A. Khademhosseini, and P. S. Doyle, "Stop-flow lithography to generate cell-laden microgel particles," Lab Chip, vol. 8, no. 7, pp. 1056-61, Jul, 2008.

[16] P. Hoffmann, M. Burmester, M. Langeheine, R. Brehm, M. T. Empl, B. Seeger, and G. Breves, "Caco-2/HT29-MTX co-cultured cells as a model for studying physiological

properties and toxin-induced effects on intestinal cells," PLoS One, vol. 16, no. 10, pp. e0257824, 2021.
[17] I. Rehor, S. van Vreeswijk, T. Vermonden, W. E. Hennink, W. K. Kegel, and H. B. Eral, "Biodegradable Microparticles for Simultaneous Detection of Counterfeit and Deteriorated Edible Products," Small, vol. 13, no. 39, pp. 1701804, 2017.
[18] Y. N. Vakkipurath Kodakkadan, K. Idzakovicova, J. Sepitka, D. Ten Napel, E. Safai, P. Cigler, F. Štěpánek, and I. Rehor, "Arbitrarily-shaped microgels composed of chemically unmodified biopolymers," Biomater Sci, vol. 8, no. 11, pp. 3044-3051, Jun 7, 2020.
[19] J. Vrba, C. Maslen, J. Maxova, J. Duras, I. Rehor, and J. Mares, "An automated platform for assembling light-powered hydrogel microrobots and their subsequent chemical binding," Journal of Computational Science, vol. 55, pp. 101446, 2021/10/01/, 2021.
[20] C. A. Schneider, W. S. Rasband, and K. W. Eliceiri, "NIH Image to ImageJ: 25 years of image analysis," Nature methods, vol. 9, no. 7, pp. 671-675, 2012.
[21] A. K. Nguyen, P. L. Goering, V. Reipa, and R. J. Narayan, "Toxicity and photosensitizing assessment of gelatin methacryloyl-based hydrogels photoinitiated with lithium phenyl-2,4,6-trimethylbenzoylphosphinate in human primary renal proximal tubule epithelial cells," Biointerphases, vol. 14, no. 2, pp. 021007, May 3, 2019.
[22] A. K. Nguyen, P. L. Goering, R. K. Elespuru, S. Sarkar Das, and R. J. Narayan, "The Photoinitiator Lithium Phenyl (2,4,6-Trimethylbenzoyl) Phosphinate with Exposure to 405 nm Light Is Cytotoxic to Mammalian Cells but Not Mutagenic in Bacterial Reverse Mutation Assays," Polymers (Basel), vol. 12, no. 7, Jul 3, 2020.
[23] D. Dendukuri, P. Panda, R. Haghgooie, J. M. Kim, T. A. Hatton, and P. S. Doyle, "Modeling of Oxygen-Inhibited Free Radical Photopolymerization in a PDMS Microfluidic Device," Macromolecules, vol. 41, no. 22, pp. 8547-8556, 2008/11/25, 2008.
[24] H. Z. An, H. B. Eral, L. Chen, M. B. Chen, and P. S. Doyle, "Synthesis of colloidal microgels using oxygen-controlled flow lithography," Soft Matter, vol. 10, no. 38, pp. 7595-7605, 2014.
[25] E. A. Kamoun, and H. Menzel, "Crosslinking behavior of dextran modified with hydroxyethyl methacrylate upon irradiation with visible light—Effect of concentration, coinitiator type, and solvent," Journal of Applied Polymer Science, vol. 117, no. 6, pp. 3128-3138, 2010.
[26] W. N. E. van Dijk-Wolthuis, J. A. M. Hoogeboom, M. J. van Steenbergen, S. K. Y. Tsang, and W. E. Hennink, "Degradation and Release Behavior of Dextran-Based Hydrogels," Macromolecules, vol. 30, no. 16, pp. 4639-4645, 1997/08/01, 1997.
[27] G. Odian, Principles of Polymerization, 4th ed.: Wiley-Interscience, 2004.
[28] M. R. Ralph H. Colby, Polymer Physics, USA: Oxford University Press, 2003.
[29] T. Canal, and N. A. Peppas, "Correlation between mesh size and equilibrium degree of swelling of polymeric networks," J Biomed Mater Res, vol. 23, no. 10, pp. 1183-93, Oct, 1989.
[30] T. Y. Lee, C. A. Guymon, E. S. Jönsson, and C. E. Hoyle, "The effect of monomer structure on oxygen inhibition of (meth)acrylates photopolymerization," Polymer, vol. 45, no. 18, pp. 6155-6162, 2004/08/19/, 2004.
[31] C. J. De Groot, M. J. Van Luyn, W. N. Van Dijk-Wolthuis, J. A. Cadée, J. A. Plantinga, W. Den Otter, and W. E. Hennink, "In vitro biocompatibility of biodegradable dextran-based hydrogels tested with human fibroblasts," Biomaterials, vol. 22, no. 11, pp. 1197-203, Jun, 2001.
[32] S. Kurata, K. Morishita, T. Kawase, and K. Umemoto, "Cytotoxic effects of acrylic acid, methacrylic acid, their corresponding saturated carboxylic acids, HEMA, and hydroquinone on fibroblasts derived from human pulp," Dent Mater J, vol. 31, no. 2, pp. 219-25, 2012.